Research Article – Vol. 02, Issue 04, No. 08

Advanced in Engineering and Intelligence Systems

Journal Web Page: https://aeis.bilijipub.com

Optimizing Pile Bearing Capacity Prediction Using Specific Random Forest Models optimized by Meta-Heuristic Algorithms for Enhanced Geomechanically Applications

Nengyuan Chen [1,2,3,*]

[1] *School of Highway, Changan University, Xi'an 710064, China*
[2] *China DK Comprehensive Investigate and Design Research Institute Co., Ltd, Xi'an 710054, China*
[3] *Shaanxi Province Soil Engineering Technology Research Center, Xi'an, Shanxi 710054, China*

Highlights

- Implementation of Specific Random Forest models enhanced with Snake Optimizer and Equilibrium Optimizer for accurate Pile Bearing Capacity (PBC) predictions.
- Validation through comprehensive analysis using soil samples from diverse types and previous stabilization tests.
- Presentation of three distinct models contributing to improved accuracy in PBC predictions.
- Notable advancements in geomechanically applications with significant implications for prediction techniques.
- Synergistic combination of specific models and meta-heuristic algorithms, demonstrating exceptional performance, with the model achieving an R2 value of for the entire dataset.

Article Info

Received: 23 November 2023
Received in revised: 25 December 2023
Accepted: 30 December 2023
Available online: 31 December 2023

Keywords

Pile Bearing Capacity;
Random Forest;
Snake Optimizer;
Equilibrium Optimizer

Abstract

To achieve highly accurate predictions of Pile Bearing Capacity (PBC), the study employs a cutting-edge approach featuring Specific Random Forest (RF) prediction models, strategically enhanced with two potent meta-heuristic algorithms: the Snake Optimizer (SO) and the Equilibrium Optimizer (EO). The effective incorporation of meta-heuristic algorithms establishes a strong basis for significantly enhancing the accuracy and effectiveness of PBC estimation. To validate the effectiveness of this model, a comprehensive analysis is conducted, leveraging PBC samples gathered from diverse soil types derived from previously conducted stabilization tests. The results of this research unveil three distinct models: RFEO, RFSO, and an individual RF model. Each of these models imparts invaluable insights, enhancing the accuracy of PBC predictions. This study not only presents an efficient and time-saving methodology but also holds significant implications for various geomechanically applications, marking a notable advancement in PBC prediction techniques. The input variables of this study can be defined as Average Cohesion, Average Friction Angle, Average Soil Specific Weight, Average Pile-Soil Friction Angle, Flap Number, Pile Area, and Pile Length. The synergistic combination of specific RF models with meta-heuristic algorithms yields auspicious outcomes, paving the way for real-time PBC estimation across a broad spectrum of geological scenarios. Remarkably, the RFSO model exhibits exceptional performance, achieving an R2 value of 0.998 for the entire dataset while boasting the lowest RMSE of 109.43. Compared to the basic RF and RFEO models, the RFSO model consistently demonstrates superior predictive and generalization capabilities.

Commented [G1]:

Commented [G2]:

Nomenclature

Indices		*ML*	*Machine learning*
PBC	*Pile bearing capacity*	*SO*	*Snake optimizer*
RF	*Random forest*	*MDAPE*	*Median absolute percetage error*
EO	*Equilibrium optimizer*	*MAE*	*Mean square error*
SO	*Snake optimizer*	*SMAPE*	*Symmetric mean absolute percentage error*

* Corresponding Author: Nengyuan Chen
Email: cnnny@aliyun.com

AI	*Artifical intelligence*	*GE*	*Geotechnical engineering*
ANNS	*Artifical neural networks*	***Parameters***	
		R^2	*Correlation coeficient*

1. Introduction

Within foundation design, figuring out the precise bearing capacity of each driven pile is crucial. While applying the same bearing capacity equation to various piles in comparable geotechnical conditions, caution should be exercised when using this method[1]– [4]. This is due to the complexity and incomplete understanding of the interaction between the pile and the soil, which causes most existing methods only to be somewhat accurate in predicting pile-bearing capacity [5]. These methods' limitations in interpreting pile behavior can be attributed to the presumptions and simplifications they are built upon[6]. The capacity of different piles within a project can frequently be determined using one of the static methods available to determine base resistance.

On the other hand, dynamic equations and methods that frequently rely on pile and hammer data, as well as pile set information to predict oversimplify the pile driving process and inadequately consider soil characteristics. Even though static tests are the most reliable approach, they have drawbacks[7], [8]. If pile loading is stopped before failure, interpreting test results cannot be easy. If loading continues until the pile fails, the test piles are damaged, limiting the applicability of this method to a small portion of all piles[9]–[11]. Therefore, there is an urgent need for a method that is affordable and capable of calculating each driven pile's precise compressive bearing capacities. Considering the wide range of variables influencing, effective computational algorithms that take into account how these variables interact are crucial. Artificial Intelligence techniques, for example, offer promising solutions in this situation because they do not rely on predefined assumptions[12]–[15].

In forecasting PBC, Artificial Neural Networks (ANNs) and various AI algorithms inspired by the structure and functioning of the human brain have become indispensable tools[16]–[18]. They are now widely used in many fields of science and engineering, particularly Geotechnical Engineering. The ability of Machine Learning techniques to analyze complex datasets and find patterns that conventional methods might miss has been extensively used in predicting. A new era of improved precision and effectiveness in predicting has arrived as a result of the integration of hand. The use of is one notable application of in this context[19]–[22]. These networks are designed to emulate the interconnected neurons in the human brain and have proven highly effective in modeling the complex relationships between soil properties, pile characteristics, and bearing capacity. Research in this field has demonstrated the remarkable precision with which can predict, establishing them as a preferred choice for. Additionally, ensemble methods have been used to predict. To increase accuracy, these algorithms combine predictions from various models. provide accurate estimates of by utilizing the combined insights of various decision trees. In conclusion, the prediction of has been transformed by and AI models, such as and ensemble techniques[23], [24]. are able to make more accurate and reliable assessments thanks to their capacity for processing complex data and uncovering intricate patterns, which ultimately results in safer and more effective construction methods.

This study presents a pioneering approach at the intersection of machine learning (ML), artificial intelligence (AI), and geotechnical engineering (GE) to enhance the accuracy and predictive capabilities of models. The employed hybridization technique is meticulously designed to optimize the performance of Random Forest (RF) models, establishing a foundation for reliable results. These hybrid models, integrating the Snake Optimizer (SO) and the Equilibrium Optimizer (EO), surpass conventional methodologies by harnessing the strengths of two advanced optimization techniques. The study systematically evaluates the models using rigorous comparisons, including metrics such as R2, MAE, RMSE, SMAPE, and MDAPE to ensure their effectiveness. This meticulous approach mitigates potential biases, providing a more precise assessment of the models' capabilities. Beyond theoretical advancements, the study also explores the practical implications of these findings in real-world geotechnical engineering applications. The demonstrated improvement in accuracy suggests the potential for these hybrid models to significantly enhance decision-making processes in geotechnical engineering projects, thereby reducing the inherent risks associated with inaccurate estimations of PBC. The Snake Optimizer (SO) and Equilibrium Optimizer (EO) offer distinct advantages in optimization. SO mimics the efficient hunting behavior of snakes, enhancing exploration-exploitation balance. EO is inspired by the equilibrium in nature, promoting convergence speed. Integrating both harnesses their complementary strengths, contributing to superior optimization outcomes in diverse applications.

2. Materials and Methodology

2.1. Data gathering

A comprehensive assessment of Pile Bearing Capacity in a soil context demands a meticulous consideration of multiple factors, and to streamline this analysis, the study thoughtfully partitioned the dataset into three distinct

subsets: training, validation, and testing. This research builds upon a dataset comprising experimental samples gleaned from prior studies, which not only serves to validate the empirical distribution method but also bolsters the predictive models employed. Leveraging the Random Forest model, this study delves into behavior by harnessing the inherent predictive prowess of the variables outlined in Table. The data collection process for prediction entails the assimilation of information from diverse sources, with a specific focus on seven critical input variables: Average Cohesion, Average Friction Angle, Average Soil Specific Weight, Average Pile-Soil Friction Angle, Flap Number, Pile Area, and Pile Length. For instance, Flap number is a unique number reflexing the condition of soil and the interactions between soil and pile which depends upon the type of the given test hammer. Also, The Pile-Soil Friction Angle represents the resistance between a pile and the surrounding soil, crucial for the stability of pile foundations. These variables provide a holistic view, encompassing a gamut of soil scenarios and conditions that impact pile behavior and bearing capacity[25]. The primary objective in amassing this data is establishing an all-encompassing and representative dataset, facilitating the training and assessment of predictive models, and yielding precise estimates[26]. Fig. visually presents the frequency distribution of each variable through a histogram plot.

Table 1. The statistic properties of the input variable of PBC.

Variables	Indicators				
	Category	*Min*	*Max*	*Avg*	*St. Dev.*
Average Cohesion (kN/m^2)	*Input*	0.00	475.00	93.08	83.66
Average Friction angle (°)	*Input*	0.00	39.00	19.97	15.35
Average soil Specific weight (kN/m^2)	*Input*	0.00	55.51	7.23	7.71
Average Pile-Soil friction angle (°)	*Input*	0.00	41.00	15.21	13.77
Flap Number	*Input*	0.00	2291.00	214.28	464.36
Pile Area (m^2)	*Input*	0.01	35.72	3.10	6.25
Pile Length (m)	*Input*	3.00	207.00	22.57	19.10
Pile Capacity (KN)	*Output*	480.00	9350.00	2723.35	1836.33

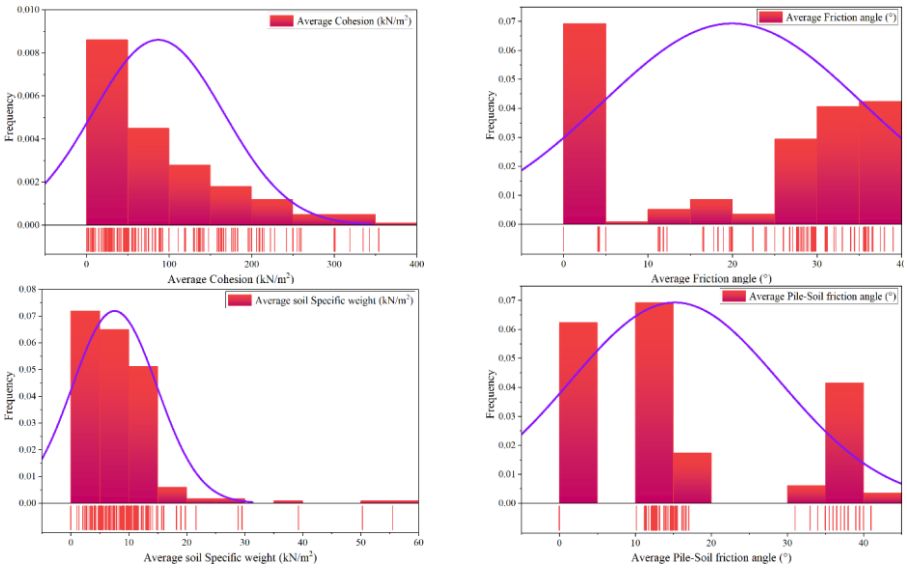

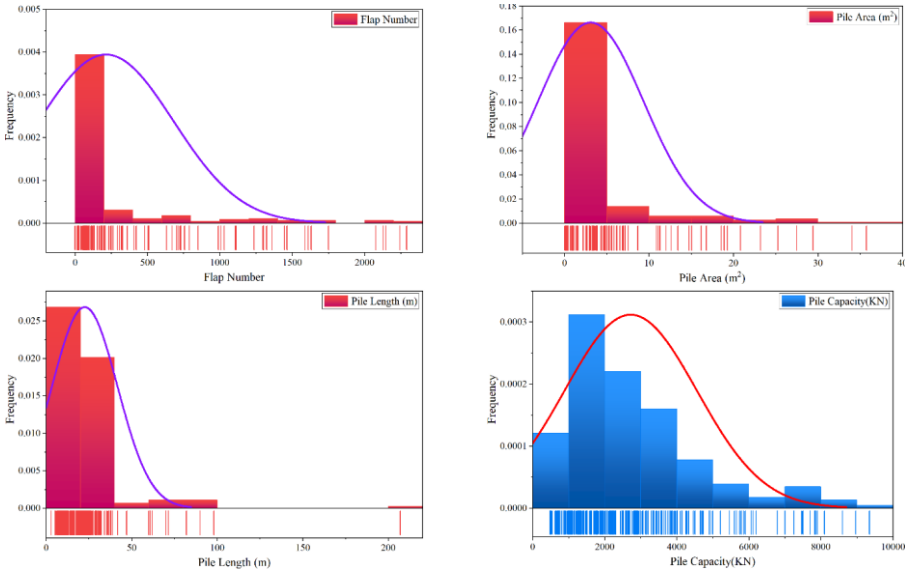

Fig. 1. The histogram-distribution plot for input and output.

Correlation between input and output parameters is illustrated in Figure 2. According to this figure, if Flap Number, Pile Area, and Pile Length possess a higher amount, it will result in higher PBC values. A higher Average Cohesion, and Average Pile-Soil Friction Angle amounts decrease the values of PBC. In summary, the input parameters can all impact the PBC. By optimizing these parameters, the desired properties and performance of the PBC will be achievable.

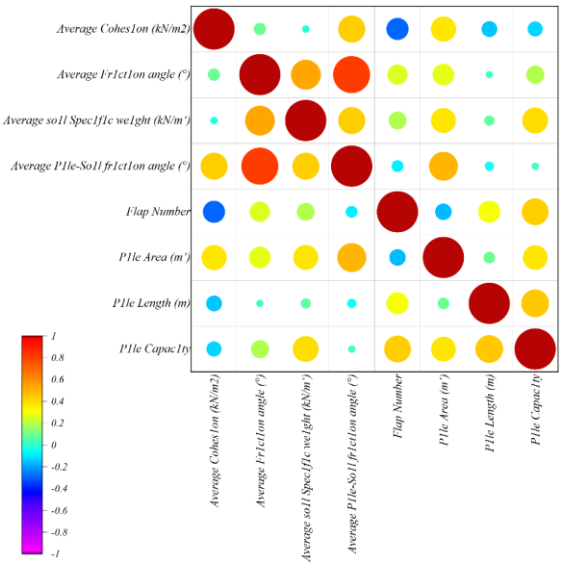

Fig. 2. The correlation between input and output parameters.

2.2. Random forest (RF)

2.2.1. Principle of RF

A random forest classifier consists of a set of tree-structured classifiers represented as $\{b(x, \aleph_l), q = 1, \dots\}$, with each tree making a unit vote to determine the most popular class for a given input x. Here, the $\{\aleph_l\}$ denote independent identically distributed random vectors. A random forest consists of multiple tree-structured classifiers developed using a training sample set and a random variable, $\{\aleph_l\}$, for the $q - th$ tree in Breiman's model [27]. The random variables are independent and identically distributed between any two trees, resulting in the creation of a classifier $b(x, \aleph_l)$, where x represents the input vector. By running the algorithm l times, a sequence of classifiers $\{b_1(x), b_2(x), \dots, b_q(x)\}$ is generated, which can be utilized to create multiple classification models. A standard majority vote determines the final output of the system, and the decision function is calculated accordingly.

$$B_{(x)} = argmax_p \sum_{i=1}^{q} F(b_i(x) = V) \quad (1)$$

Each tree has the right to vote for the best classification result for a given input variable, and the combination of these individual decision tree models is denoted as $B(x)$. The output variable is V, and the indicator function is represented as $F(.)$ [28].

2.2.2. Characters of RF

The margin function [29], which is employed in RF to assess the extent by which the average number of votes for the correct class at X, V, surpasses that for the incorrect class, can be defined as:

$$mc(X, V) = av_l F(b_l(X) = V) - max_{j \neq V} av_l F(b_l(X) = j) \quad (2)$$

The margin function gauges the precision and assurance of the classification prediction, with a more significant value denoting heightened accuracy and confidence [30]. The generalization error for this classifier can be defined as:

$$OS^* = O_{X,V}(mc(X, F) < 0) \quad (3)$$

Leo Breiman established that the random variable $b_q(X) = b(x, \aleph_q)$, follows the Strong Law of Large Numbers when the number of decision trees is sufficiently large. As the number of decision trees increases, $OS*$ converges to a specific value for almost all sequences of $\aleph_1$ Breiman also demonstrated that RF is not susceptible to overfitting and can yield a limiting value for the generalization error.

$$O_{x,V}(O_\theta(b_l(x,\theta)=V)-max_{j\neq V}O_\theta(b(x,\theta)=j)<0) \quad (4)$$

Leo Breiman's work also established an upper bound for the generalization error.

$$OS^* \leq \bar{\beta}(1-z^2)/z^2 \quad (5)$$

Two factors that influence the generalization error of RF are the strength of each tree in the forest, denoted by (z), and the correlation between the trees, represented by the average correlation value $\bar{\beta}$. A lower correlation value indicates reduced interdependence between the trees, which results in improved performance for the RF [31].

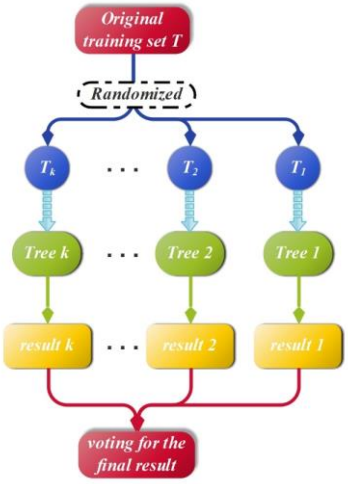

Fig. 3. The flowchart of the RF method

2.3. Snake optimizer (SNO)

The snakes' mating rituals serve as an inspiration for the SNO algorithm. The search process is divided into two phases based on this information: exploitation and exploration [32].

2.3.1. Initialize

As with all metaheuristic algorithms, SNO initiates by creating a uniform random population to kickstart the optimization process. The following equation yields the initial population:

$$x_i = x_{min} + rand \times (x_{max} - x_{min}) \quad (6)$$

The position of the ith individual, x_i, can be determined using the equation, where $rand$ is a random number between 0 and 1, and x_{max} and x_{min} represent the upper and lower bounds of the problem, alternatively.

2.3.2. Search Phase

When F is less than 0.25, the snake explores by adjusting its position based on its current location and selecting a random point. To model food quality, temperature, and the search phase, the following calculations can be employed:

$$F = s_1 \times \exp\left(\frac{r-R}{R}\right) \quad (7)$$

$$\text{Temp} = \exp\left(\frac{-r}{R}\right) \quad (8)$$

$$X_i(t+1) = X_{rand}(t) \pm s_2 \times B \times ((X_{max} - X_{min}) \times rand + X_{min}) \quad (9)$$

In the context presented, the constants s_1 and s_2 are defined as 0.5 and 0.05, respectively. Here, r represents the current repetition, while R signifies the maximum number of repetitions. Additionally, X_{rand} denotes the randomly determined position, and $rand$ signifies a randomly

generated number ranging from 0 to 1. The ability to locate food, denoted as B, is further elaborated as follows:

$$B = \exp\left(\frac{-q_{rand}}{q_i}\right) \quad (10)$$

In this context, q_{rand} represents the fitness of X_{rand}, while q_i denotes the fitness of the individual at the $i-th$ position.

2.3.3. Exploitation phase

When both F is higher than 0.25 and the temperature exceeds 0.6, the snake's movement will be exclusively directed towards the food source. This movement can be quantified through the following calculation:

$$X_{i,j}(t+1) = X_{food} \pm s_3 \times M \times rand \times (X_{food} - X_{i,j}(t)) \quad (11)$$

In this context, $X_{i,j}$ represents the position of the snake, X_{food} denotes the optimal position and s_3 corresponds to a constant value of 2. When the temperature falls below 0.6, the snake enters either the fight mode or the mating mode, which can be defined as per Eq. (12):

$$X_i(t+1) = X_i + s_3 \times A \times rand \times (F \times X_{best} - X_i(t)) \quad (12)$$

In this scenario, X_i refers to the position at the $i-th$ iteration, X_{best} signifies the most optimal position, and A represents the capability to engage in combat. The computation of A can be expressed as follows:

$$A = \exp\left(\frac{-q_{best}}{q_i}\right) \quad (13)$$

In this context, q_{best} represents the highest fitness value, while q_i denotes the fitness of the individual. The process of mating mode can be determined through the following calculation:

$$X_i(t+1) = X_i + s_3 \times G \times rand \times (F \times X_i(t)) \quad (14)$$

In this context, G represents the mating capability. This can be quantified using the following calculation:

$$G = \exp\left(\frac{-q_i}{q_i}\right) \quad (15)$$

Upon successful egg hatching, the protocol involves selecting the least proficient snake and replacing it:

$$X_{worst} = X_{min} + rand \times (X_{max} - X_{min}) \quad (16)$$

Here, the worst individual is indicated by X_{worst}.

The directional flag operator $\pm$, often referred to as the diversity factor, possesses the capacity to enhance or diminish the positional solution, thereby increasing the likelihood of the agent altering its direction and effectively exploring the given space from various perspectives. This parameter is of the utmost importance in meta-heuristic algorithms, which are inherently built to include randomness for enhanced diversification.

2.4. Equilibrium Optimizer (EO)

The well-mixed dynamic equilibrium analysis solution within the control volume was the basis for the Equilibrium Optimizer (EO). The EO optimization procedure, like some other modern algorithms, can unintentionally create a population in the various dimensions of the search area for the optimizations matters, where the particles are the solutions and the concentration acts as the positions of the particles [32]. Along with the uniform random initialization of the first accumulations, the searching area and population dimensions can be introduced in the following ways depending on the particle count [33]:

$$C_d^k = C_d^{min} + \left(C_d^{max} - C_d^{min}\right) \times rand_d^k \quad k = 1,2,\dots,m \quad (17)$$

The four candidates lead the EO to improve the exploring phase, while others support the exploiting stage [34].

$$C_{e,pool} = \{C_{e,1}, C_{e,2}, C_{e,3}, C_{e,4}, C_{e,pool}\} \quad (18)$$

In iterations, the particle density would be updated accidentally among the chosen candidates with a similar probability of selection. Nevertheless, for the iteration first, the initially opted particle updates all concentrations corresponded to C. Afterward, in the next epoch, the concentrations of the similar particles can be upgraded according to $C_{e,mean}$. The updated process repeats for particles until the end of the process. The exponential variable of U assists the concentrating update principal to achieve the proper equilibrium among exploration and exploitation, calculated as follows.

$$U = \exp\left(-v(t - t_0)\right) \quad (19)$$

The t value declined if the number of iterations went up.

$$t = \left(1 - itr/maxitr\right)^{(h_2 \times itr/maxitr)} \quad (20)$$

$$t_0 = t + 1/\mathrm{v} \times \ln\left(-h_1 sign(r_1 - 0.5)[1 - \exp(-\mathrm{v}t)]\right) \quad (21)$$

In this regard, the term $(r_1 - 0.5)$ affects exploitation and exploration phases. The following equation must be considered to improve the ability to exploit and explore convergence ensuring. Moreover, for improving the exploiting stage, the generation rate is progressed as the

primary step in the EO algorithm process that provides optimal solutions.

$$G = \mathrm{GRC} \times (C_e - \mathrm{v}C) \times \exp\left(-\delta(t - t_0)\right) \quad (22)$$

$$GRC = \begin{cases} 0.5r_2 & if \quad r_3 \geq GP \\ 0 & if \quad r_3 \leq GP \end{cases} \quad (23)$$

The rule of update for EO can obtained by Eq. (24).

$$C = C_e + (C - C_e)\,\mathrm{U} + \mathrm{G} \times 1/\mathrm{v} \times (1 - U) \quad (24)$$

The fittest value of every particle in the current iteration is compared to an identical value in the previous iteration and will be stored if it results in an improved value. This procedure assists the ability of exploitation but may raise the chance of falling in local minima if the technique does not achieve benefit from the ability of global exploration. More details of the EO algorithm is reported in.

2.5. Performance evaluation methods

This article uses a variety of metrics to assess the models, including the previously mentioned Median Absolute Percentage Error ($MDAPE$), Correlation Coefficient (R^2), Mean Square Error (MAE), Symmetric Mean Absolute Percentage Error ($SMAPE$), and Root Mean Square Error ($RMSE$). Excellent performance of the algorithm during the phases of training, validation, and testing is indicated by a high R^2 value. On the other hand, lower $RMSE$ and MAE values are preferable because they show less model error. Eqs. $(25-29)$ are used to calculate these metrics.

$$R^2 = \left(\frac{\sum_{i=1}^{W} (h_i - \bar{h})(q_i - \bar{q})}{\sqrt{[\sum_{i=1}^{W} (h_i - h)^2][\sum_{i=1}^{W} (q_i - \bar{q})^2]}} \right)^2 \quad (25)$$

$$RMSE = \sqrt{\frac{1}{W} \sum_{i=1}^{W} (q_i - h_i)^2} \quad (26)$$

$$MAE = \frac{1}{W} \sum_{i=1}^{W} |q_i - h_i| \quad (27)$$

$$SMAPE = \frac{100}{W} \sum_{i}^{W} \frac{2 \times |q_i - h_i|}{|q_i| + |h_i|} \quad (28)$$

$$MDAPE = 100 \times median\left(\frac{|q_i - \bar{q}|}{|h_i - \bar{h}|} \right) \quad (29)$$

In these equations, h_i and q_i refer to the predicted and experimental values, respectively. The mean values of the experimental samples and predicted are represented by $\bar{h}$ and $\bar{q}$. Alternatively, W denotes the number of samples being considered.

3. Result and Discussion

In the context of machine learning, hyperparameters are parameters that are pre-defined before the training process and remain constant during the training phase. This research set up the optimizers by specifying hyperparameters such as n_estimators, max_depth, and min_samples_split. By tuning these hyperparameters effectively, it is feasible to enhance the performance of the optimizer and avoid problems such as underfitting or overfitting of the model. Consequently, selecting suitable hyperparameters is essential in building a dependable and precise machine-learning model.

Table 2. The results of hyper parameters for RF.

Models	Hyper parameter		
	n_estimators	max_depth	min_samples_split
RF	100	None	2.00E+00
RFSO	409	877	19
RFEO	710	47	49

The study's objective was to make predictions for PBC using three distinct models: RF, $RFSO$, and $RFEO$. To ensure an unbiased assessment of these models' performance, the study divided experimental measurements into three phases, as shown in Table 2: training (70%), validation (15%), and testing (15%). To comprehensively evaluate and compare these algorithms, the study employed five statistical metrics: R^2, $RMSE, MDAPE, SMAPE$, and MAE.

- The primary focus of model evaluation was on the R^2 values, which indicate how well the independent variable explains the variance in the dependent variable. During the training phase, the $RFSO$ model exhibited exceptional predictive accuracy, achieving the highest R^2 value of 0.998 among all models, surpassing the others. In contrast, the RF

model displayed slightly lower R^2 values of 0.985 during the training phase.

- Furthermore, the study examined other error indicators, including *RMSE*, which ranged from 109.43 to 261.87. Notably, the *RFSO* model demonstrated the lowest errors, while the *RF* model had the highest.
- Additionally, the study considered the *MDAPE* value, with the *RF* model having the highest value of 6.591 during the training phase, while the *RFSO* model had the lowest value of 2.665 during the same phase.
- For *MAE* and *SMAPE*, the *RF* model had the highest and least favorable values during the training phase (*MAE*: 193.70), and the *RFEO* model also had the highest and least favorable value during the training phase (*SMAPE*: 0.0004).

Overall, the results indicate that the *RFSO* model outperformed the *RF* and *RFEO* models in particular phases. However, when choosing a model for real-world applications, it is essential to consider other factors such as model complexity, computational efficiency, and ease of implementation.

Table 3. Performance indices of proposed models

Models	**RF**			**RFSO**			**RFEO**		
Section	**Train**	**Validation**	**Test**	**Train**	**Validation**	**Test**	**Train**	**Validation**	**Test**
RMSE	261.87	370.32	395.02	109.43	216.61	220.55	225.71	369.28	363.35
R^2	0.985	0.976	0.952	0.998	0.995	0.990	0.993	0.988	0.975
MAE	193.70	254.02	295.78	82.88	153.41	168.60	173.69	262.96	288.47
SMAPE	0.0004	0.0025	0.0030	0.0001	0.0015	0.0017	0.0004	0.0026	0.0030
MDAPE	6.591	9.074	9.635	2.665	4.649	5.862	6.023	8.930	11.024

Fig. 4 presents a scatter plot illustrating the performance of hybrid models across the three stages of training, validation, and testing. The assessment relies on two crucial criteria, namely R^2 and *RMSE*. R^2 quantifies the agreement between predicted and observed values, while *RMSE* characterizes the extent of dispersion or prediction error. In the case of the *RFSO* model, the data points are closely grouped around the central line, indicating its exceptional accuracy across all three phases. The tight clustering between predicted and actual values signifies minimal dispersion and a high level of agreement. In contrast, the *RFEO* and *RF* models exhibit a more evenly spread distribution of data points around the central line, suggesting comparable performance levels. However, compared to the *RFSO* model, this broader dispersion implies a higher degree of error and somewhat reduced accuracy.

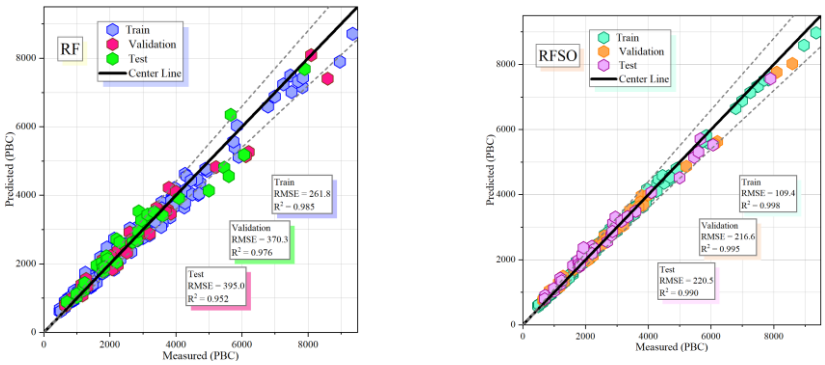

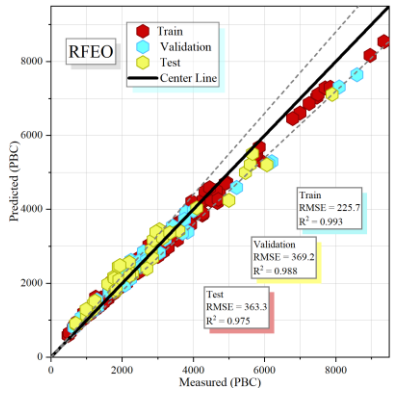

Fig. 4. The scatter plot for developed hybrid models.

Using a line plot in Fig. 5, this study compares expected and observed PBC. Training, validation, and testing comprise these graphical representations three main sections. The model's accuracy depends on how well the expected behavior matches the observed behavior. The measured values for these three phases differ slightly from one another. Notably, this divergence is caused by the $RFSO$ model having the highest proportion of predicted points higher than measured points. The predicted and measured points of the RF and $RFEO$ models exhibit some variance, but their precision is slightly lower than that of the $RFSO$ model.

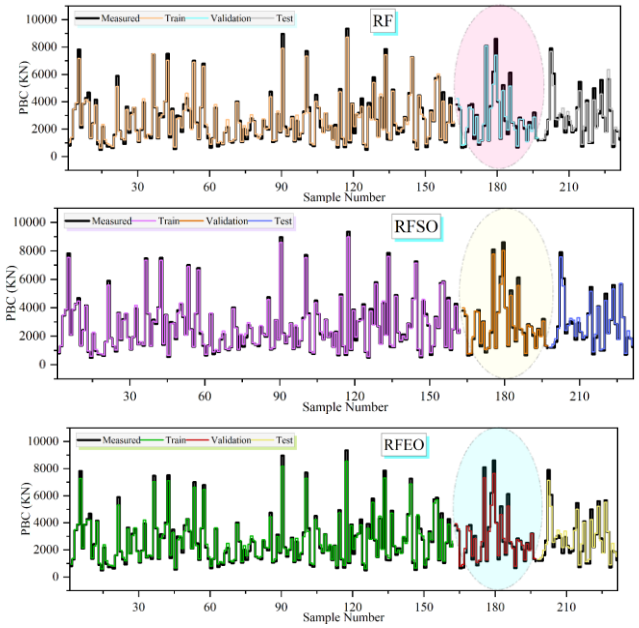

Fig. 5. The comparison of measured and predicted values.

A histogram-density plot, as seen in Fig. 6, displays the distribution of error percentages among the presented models during the aforementioned training, validation, and testing phases. Remarkably, the *RFSO* model demonstrated impressive accuracy, maintaining the lowest error rates throughout each stage, ranging from −10% to 15%. Throughout the training phases, the error rate for the *RF* model fluctuated between −20% and 30%. Despite the discrepancy, all three models displayed a commendable level of prediction accuracy.

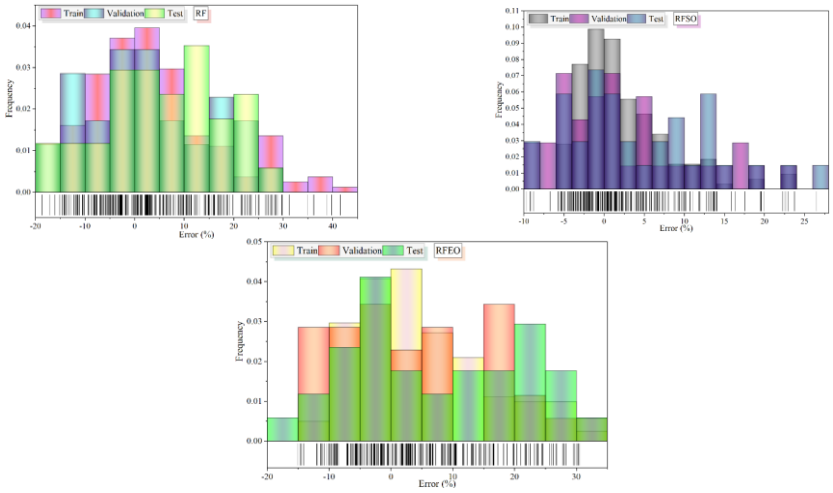

Fig. 6. The error percentage for the hybrid models is based on a histogram density plot.

In Fig. 7, a box plot illustrates the error percentages related to the models investigated in this study. Throughout the training phase, the *RFSO* model demonstrated a consistent 0% average error rate, exhibiting minimal variance. The error distribution was quite favorable, consistently remaining below the 10% threshold. In contrast, the *RF* model displayed dispersion across three distinct phases, featuring a symmetric and evenly distributed standard curve. However, the model kept its error percentage within the 20% range. On the other hand, *RFEO* exhibited the most notable and diverse deviations. An extraordinary outlier data point during the evaluation phase accounted for more than 20% of the dataset, an uncommon occurrence in statistical analysis.

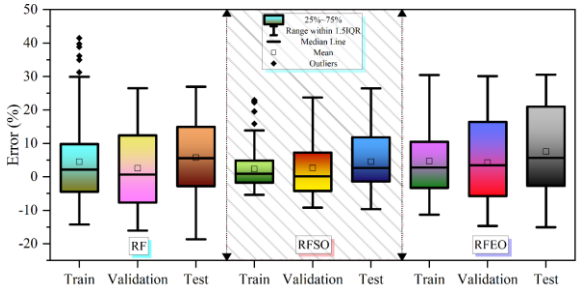

Fig. 7. The box plot of errors among the developed models.

4. Conclusion

A significant and complex challenge in pile analysis and design is to predict the ultimate bearing capacity of piles (PBC) using field experimental data and AI techniques. The goal of this research is to develop innovative AI predictive models for PBC estimation. To achieve this goal, the current study uses the Random Forest (RF) model and cutting-edge ML techniques to forecast PBC. Two meta-heuristic algorithms, the Snake Optimizer (SO) and the Equilibrium Optimizer (EO), are seamlessly integrated to improve the predictive performance of the RF model. By conducting an exhaustive evaluation encompassing various performance assessment metrics detailed in the corresponding section, this study quantifies these models' effectiveness and predictive capabilities in estimating PBC properties. The ensuing results emanate from this meticulous evaluation process.

1. This study showed that the $RFSO$ models had the highest R2 values and the RF model had the lowest R2 values, despite the difference being only 1.2%.
2. Surprisingly, with a staggering 79% decrease from the RF values, the $RMSE$ values for the $RFSO$ models consistently emerged as the most impressive.
3. According to the error indicators, the $RFSO$ models performed better than the RF and $RFEO$ models, showing lower error values.
4. The SO optimizer and RF combination was highly successful in achieving high accuracy in predicting PBC based on this noteworthy result.
5. This study presents a novel ML and AI model for predicting PBC mechanical properties, with potential applications in the engineering and building sectors.

REFERENCES

[1] K. Chatterjee, D. Choudhury, and H. G. Poulos, "Seismic analysis of laterally loaded pile under influence of vertical loading using finite element method," *Comput Geotech*, vol. 67, pp. 172–186, 2015.

[2] M. A. Benbouras, A.-I. Petrişor, H. Zedira, L. Ghelani, and L. Lefilef, "Forecasting the bearing capacity of the driven piles using advanced machine-learning techniques," *Applied Sciences*, vol. 11, no. 22, p. 10908, 2021.

[3] H. Maizir and K. A. Kassim, "Neural network application in prediction of axial bearing capacity of driven piles," in *Proceedings of the international multiconference of engineers and computer scientists*, 2013, pp. 13–15.

[4] F. P. Nejad, M. B. Jaksa, M. Kakhi, and B. A. McCabe, "Prediction of pile settlement using artificial neural networks based on standard penetration test data," *Comput Geotech*, vol. 36, no. 7, pp. 1125–1133, 2009.

[5] A. Elgamal, A. Elnimr, A. Ahmed Dif, and A. Gabr, "Prediction of Pile Bearing Capacity Using Artificial Neural Networks.," *MEJ-Mansoura Engineering Journal*, vol. 37, no. 3, pp. 1–14, 2021.

[6] M. Khanmohammadi, D. J. Armaghani, and M. M. Sabri Sabri, "Prediction and Optimization of Pile Bearing Capacity Considering Effects of Time," *Mathematics*, vol. 10, no. 19, p. 3563, 2022.

[7] B. R. Murlidhar, R. K. Sinha, E. T. Mohamad, R. Sonkar, and M. Khorami, "The effects of particle swarm optimisation and genetic algorithm on ANN results in predicting pile bearing capacity," *International Journal of Hydromechatronics*, vol. 3, no. 1, pp. 69–87, 2020.

[8] L. Gabrielaitis, V. Papinigis, and G. Žaržojus, "Estimation of settlements of bored piles foundation," *Procedia Eng*, vol. 57, pp. 287–293, 2013.

[9] J. Wang, Z. Zhou, H. Fu, Q. Dong, Y. Cai, and X. Hu, "Influence of vacuum preloading on vertical bearing capacities of piles installed on coastal soft soil," *Marine Georesources & Geotechnology*, vol. 37, no. 7, pp. 870–879, 2019.

[10] W. Chen, P. Sarir, X.-N. Bui, H. Nguyen, M. M. Tahir, and D. Jahed Armaghani, "Neuro-genetic, neuro-imperialism and genetic programing models in predicting ultimate bearing capacity of pile," *Eng Comput*, vol. 36, pp. 1101–1115, 2020.

[11] T. A. Pham, H.-B. Ly, V. Q. Tran, L. Van Giap, H.-L. T. Vu, and H.-A. T. Duong, "Prediction of pile axial bearing capacity using artificial neural network and random forest," *Applied Sciences*, vol. 10, no. 5, p. 1871, 2020.

[12] H. H. Elmousalami, "Artificial intelligence and parametric construction cost estimate modeling: State-of-the-art review," *J Constr Eng Manag*, vol. 146, no. 1, p. 03119008, 2020.

[13] L. Wang, Q. Cao, Z. Zhang, S. Mirjalili, and W. Zhao, "Artificial rabbits' optimization: A new bio-inspired meta-heuristic algorithm for solving engineering optimization problems," *Eng Appl Artif Intell*, vol. 114, p. 105082, 2022.

[14] M. Nguyen Duc, A. Ho Sy, T. Nguyen Ngoc, and T. L. Hoang Thi, "An Artificial Intelligence Approach Based on Multi-layer Perceptron Neural Network and Random Forest for Predicting Maximum Dry Density and Optimum Moisture Content of Soil Material in Quang Ninh Province, Vietnam," in *CIGOS 2021, Emerging Technologies and Applications for Green Infrastructure: Proceedings of the 6th International Conference on Geotechnics, Civil Engineering and Structures*, Springer, 2022, pp. 1745–1754.

[15] B. U. Ayhan and O. B. Tokdemir, "Safety assessment

in megaprojects using artificial intelligence," *Saf Sci*, vol. 118, pp. 273–287, 2019.
[16] S. Akbulut, E. Kalkan, and S. Celik, "Artificial Neural Networks to estimate the shear strength of compacted soil samples," in *Int Conf New Dev Soil Mech Geotech Eng*, 2003, pp. 285–290.
[17] A. T. A. Dantas, M. B. Leite, and K. de Jesus Nagahama, "Prediction of compressive strength of concrete containing construction and demolition waste using artificial neural networks," *Constr Build Mater*, vol. 38, pp. 717–722, 2013.
[18] M. R. Akbarzadeh, H. Ghafourian, A. Anvari, R. Pourhanasa, and M. L. Nehdi, "Estimating Compressive Strength of Concrete Using Neural Electromagnetic Field Optimization," *Materials*, vol. 16, no. 11, p. 4200, 2023.
[19] T. Onsree and N. Tippayawong, "Machine learning application to predict yields of solid products from biomass torrefaction," *Renew Energy*, vol. 167, pp. 425–432, 2021.
[20] Y. Liu, Y. Wang, and J. Zhang, "New machine learning algorithm: Random Forest," in *Information Computing and Applications: Third International Conference, ICICA 2012, Chengde, China, September 14-16, 2012. Proceedings 3*, Springer, 2012, pp. 246–252.
[21] L. Farahzadi and M. Kioumarsi, "Application of machine learning initiatives and intelligent perspectives for CO2 emissions reduction in construction," *J Clean Prod*, vol. 384, p. 135504, 2023.
[22] G. Carleo *et al.*, "Machine learning and the physical sciences," *Rev Mod Phys*, vol. 91, no. 4, p. 045002, 2019.
[23] R. Sarkhani Benemaran, M. Esmaeili-Falak, and H. Katebi, "Physical and numerical modelling of pile-stabilised saturated layered slopes," *Proceedings of the Institution of Civil Engineers-Geotechnical Engineering*, vol. 175, no. 5, pp. 523–538, 2022.
[24] F. Masoumi, S. Najjar-Ghabel, A. Safarzadeh, and B. Sadaghat, "Automatic calibration of the groundwater simulation model with high parameter dimensionality using sequential uncertainty fitting approach," *Water Supply*, vol. 20, no. 8, pp. 3487–3501, 2020.
[25] E. Momeni, R. Nazir, D. J. Armaghani, and H. Maizir, "Prediction of pile bearing capacity using a hybrid genetic algorithm-based ANN," *Measurement*, vol. 57, pp. 122–131, 2014.
[26] T. A. Pham and H.-L. T. Vu, "Application of ensemble learning using weight voting protocol in the prediction of pile bearing capacity," *Math Probl Eng*, vol. 2021, pp. 1–14, 2021.
[27] G. Biau and E. Scornet, "A random forest guided tour," *Test*, vol. 25, pp. 197–227, 2016.
[28] A. Sarica, A. Cerasa, and A. Quattrone, "Random Forest algorithm for the classification of neuroimaging data in Alzheimer's disease: a systematic review," *Front Aging Neurosci*, vol. 9, p. 329, 2017.
[29] W. Lin, Z. Wu, L. Lin, A. Wen, and J. Li, "An ensemble random forest algorithm for insurance big data analysis," *Ieee access*, vol. 5, pp. 16568–16575, 2017.
[30] H. Khajavi and A. Rastgoo, "Predicting the carbon dioxide emission caused by road transport using a Random Forest (RF) model combined by Meta-Heuristic Algorithms," *Sustain Cities Soc*, vol. 93, p. 104503, 2023.
[31] A. D. Kulkarni and B. Lowe, "Random Forest algorithm for land cover classification," 2016.
[32] S. Agnihotri, A. Atre, and H. K. Verma, "Equilibrium optimizer for solving economic dispatch problem," in *2020 IEEE 9th Power India International Conference (PIICON)*, IEEE, 2020, pp. 1–5.
[33] S. K. ElSayed, S. Al Otaibi, Y. Ahmed, E. Hendawi, N. I. Elkalashy, and A. Hoballah, "Probabilistic modeling and equilibrium optimizer solving for energy management of renewable micro-grids incorporating storage devices," *Energies (Basel)*, vol. 14, no. 5, p. 1373, 2021.
[34] A. Faramarzi, M. Heidarinejad, B. Stephens, and S. Mirjalili, "Equilibrium optimizer: A novel optimization algorithm," *Knowl Based Syst*, vol. 191, p. 105190, Mar. 2020, doi: 10.1016/j.knosys.2019.105190.